Intermittent Nature of Acceleration in Near Wall Turbulence

Changhoon Lee,* Kyongmin Yeo, and Jung-Il Choi†

Department of Mechanical Engineering and Yonsei Center for Clean Technology, Yonsei University, 134 Shinchon-dong, Seodaemun-gu Seoul, 120-749, Korea

(Received 1 November 2003; published 9 April 2004)

Using direct numerical simulation of a fully developed turbulent channel flow, we investigate the behavior of acceleration near a solid wall. We find that acceleration near the wall is highly intermittent and the intermittency is in large part associated with the near wall organized coherent turbulence structures. We also find that acceleration of large magnitude is mostly directed towards the rotation axis of the coherent vortical structures, indicating that the source of the intermittent acceleration is the rotational motion associated with the vortices that causes centripetal acceleration.

DOI: 10.1103/PhysRevLett.92.144502 PACS numbers: 47.27.Nz, 02.50.Fz, 02.70.Hm

Recently, it was shown that fluid particle acceleration in turbulence is extremely intermittent in the Lagrangian measurement of fluid acceleration [1,2]. The authors of [1,2] further showed that the acceleration variance is quite anisotropic even in high Reynolds number turbulence. In another Lagrangian experiment, it was reported that accelerations have random uncorrelated directions but a magnitude is extremely long range correlated in time [3]. By constructing a Langevin equation of which the solution possesses such properties, the authors of [3] claimed that long time correlation in the magnitude of acceleration is a key to intermittency in turbulence. Recent numerical studies [4,5] also revealed that acceleration variances show Reynolds number dependence. All of these reported results are in contrast with the traditional belief that the fluid particle acceleration is associated with the motion of scale smaller than the Kolmogorov scale [6]. It was suggested that the anomalous scaling of acceleration is mainly due to the pressure gradient fluctuations which have length scales larger than the Kolmogorov scale [4]. Some speculated that the characteristics of accelerations are associated with the coherent motions of fluid [2,5,7]. However, it is not clear how this motion of fluid determines acceleration characteristics.

In this Letter, we investigate behavior of acceleration in association with coherent motion of fluid using direct numerical simulation of near wall turbulence. Near wall turbulence induced by a pressure gradient is a "real" flow unlike artificially forced isotropic turbulence, and much insight into the flow physics in near wall turbulence can be gained through numerical simulations. Near wall turbulence is different from isotropic turbulence, in which tubelike vortex filaments are intermittently found [8], in that large coherent turbulence structures are found with preferred orientations very close to the wall. Among them, the most pronounced one is the streamwise vortex, which is an elongated vortical structure rotating about the axis roughly parallel with the mean flow direction [9]. Here we show that these structures are the main source of acceleration intermittency near the wall.

We carried out simulations of turbulent channel flow at $\mathrm{Re}_\tau (\equiv u_\tau \delta/\nu) = 180$ using a spectral method utilizing the Fourier and Chebyshev expansions in the homogeneous horizontal directions and the wall-normal direction, respectively. Here, u_τ, δ, and ν are the wall-shear velocity, half the channel gap, and the viscosity of fluid, respectively. The computational domain is $(4\pi, 2, 4\pi/3)\delta$ in the streamwise, wall-normal, and spanwise directions and the numerical grids are $128 \times 129 \times 128$ in respective directions. The time advancing was made using the third-order Runge-Kutta scheme combined with the Crank-Nicolson scheme. A highly accurate particle tracking algorithm employing the four-point Hermite interpolation in the horizontal directions and Chebyshev interpolation method in the wall-normal direction was used to obtain the particle trajectories and acceleration variation along a trajectory [10].

The behavior of the trajectories of fluid particles starting near the wall obtained from simulations implies the existence of a rotating structure as clearly demonstrated in Fig. 1. Acceleration several times larger than the root-mean square (rms) value is observed in one of the investigated trajectories, and extra fluid particles released in the very neighborhood all get trapped in the intertwined helical motion with large acceleration as shown in the inset of Fig. 1. This clearly indicates that large accelerations are closely related with the presence of a coherent organized structure rotating about the streamwise direction. Even more surprisingly, accelerations all direct towards the rotation axis, suggesting that the acceleration is in large part the centripetal acceleration caused by the rotational motion associated with the coherent vortical structure. In our simulated flow, large-amplitude excursion of acceleration more than 20 times larger than the rms value is always found near the edge of the coherent vortical structure, pointing toward the rotation axis.

Acceleration a_i is composed of two contributions from pressure and viscous forces.

$$a_i = a_i^I + a_i^S = -\frac{1}{\rho}\frac{\partial p}{\partial x_i} + \nu \frac{\partial^2 u_i}{\partial x_j \partial x_j}, \qquad (1)$$

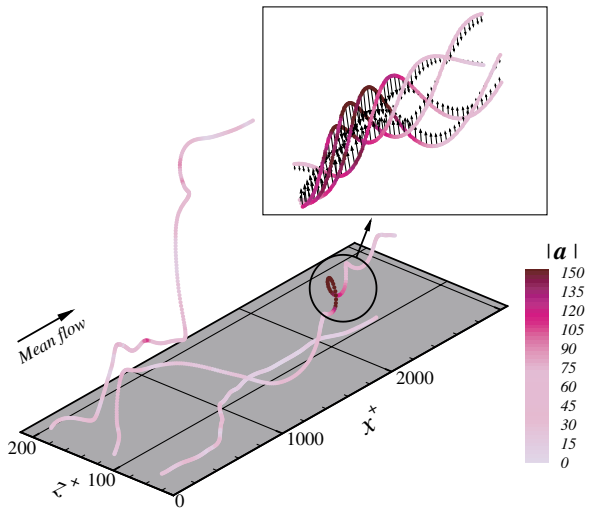

FIG. 1 (color online). Trajectories of particles released at $y^+(\equiv yu_\tau/\nu) = 15$. Contours denote the magnitude of fluid particle acceleration normalized by u_τ^2/δ with standard deviation of about 20. Vectors in the inset denote acceleration vectors.

where a_i^I is called the irrotational (or potential) component of acceleration and a_i^S the solenoidal component [4]. Here, ρ, p, and u_i are density, pressure, and velocity components, respectively. In high Reynolds number isotropic turbulence, a_i^S is usually much smaller than a_i^I [4,11]. However, this is not the case for near wall turbulence due to the presence of the wall as shown below.

The simulated root-mean square accelerations in each direction normalized by u_τ and δ as functions of the distance from the wall are illustrated in Fig. 2, in which peaks of all three components are found near the wall. The mean part of the streamwise acceleration due to the

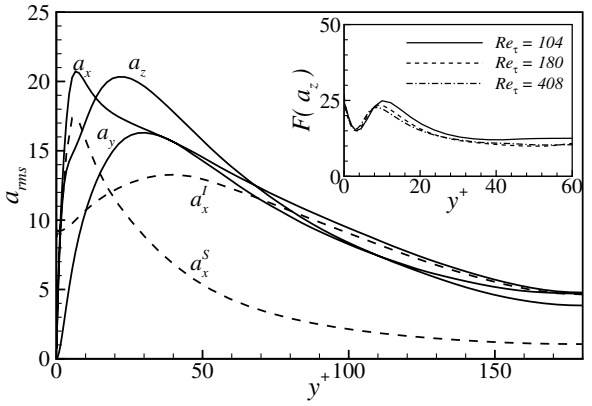

FIG. 2. Near wall root-mean square acceleration distributions against the wall-normal distance normalized by u_τ and ν. Here, x, y, and z denote the streamwise, wall-normal, and spanwise directions, respectively. The solenoidal parts of the wall-normal and spanwise accelerations are not shown since they are negligibly small. In the inset, the flatness of the spanwise acceleration components for three different Reynolds numbers is shown.

mean pressure gradient, albeit small, is subtracted from the total acceleration to yield the fluctuation part. For the streamwise component, the irrotational component and the solenoidal component are also drawn since they are comparable in magnitude. The peaks of the a_x^I, a_y, and a_z are found in comparable magnitude at $y^+ = 20$–40 where the coherent vortical structures are most frequently found. Only the wall-normal and spanwise accelerations are mostly linked to the streamwise vortex as demonstrated in Fig. 1. Moreover, investigation reveals that the streamwise acceleration almost vanishes in the core region of the streamwise vortex. It is observed that mostly a_x^I is due to slanted streamwise vortices and other coherent structures as shown below. The peak of a_x^S very near the wall is caused by the viscous interaction between the streamwise vortices and wall.

Since the coherent structures are found in a considerably intermittent manner, accelerations are also highly intermittent as shown in the inset of Fig. 2 in which the flatness defined by $F(a_i) = \overline{a}_i^4/(\overline{a}_i^2)^2$ for three different Reynolds numbers are demonstrated with the overline denoting the ensemble average. Since the flatness is a very slowly converging quantity, we used 1.3×10^9 samples to ensure convergence. A typical value of $F(a_i)$ in $y^+ = 10$–50 is about 15, which is considerably greater than the Gaussian value 3 with a somewhat surprising invariance with respect to the Reynolds number since the value measured for isotropic turbulence is much greater and shows Reynolds number dependence [1].

Sometimes it is more instructive to investigate instantaneous flow field rather than statistical data. The vortical structures near the wall visualized by a vortex identification scheme called the λ_2 method [12] are illustrated in Fig. 3, in which the contours of the streamwise component of vorticity vector ω ($\equiv \nabla \times \mathbf{u}$) are also represented in color on the surface of the structures. It is easily recognized that counterrotating two streamwise vortices are, in fact, parts of a single three-dimensional vortical structure known as a horseshoe or hairpin vortex, which is another frequently observed structure in near wall turbulence [13]. Section A of the leg part of the structure clearly shows a strong streamwise vorticity core with all accelerations in the neighborhood converging towards the center of it (inset A to Fig. 3). Similarly, in section B of the arch of the hairpin vortex, the spanwise vorticity core is found with acceleration containing the wall-normal and streamwise components pointing to the center of it (inset B of Fig. 3). Since the leg part of the hairpin vortex is slightly slanted outward in the streamwise direction, the arch of the vortex is found a little farther away from the wall than the legs. This is why the irrotational component of the streamwise acceleration of comparable magnitude to other components has a peak at a slightly different distance from the wall in Fig. 2.

The helical motions of fluid particles (Fig. 1) and acceleration distribution near the coherent near wall

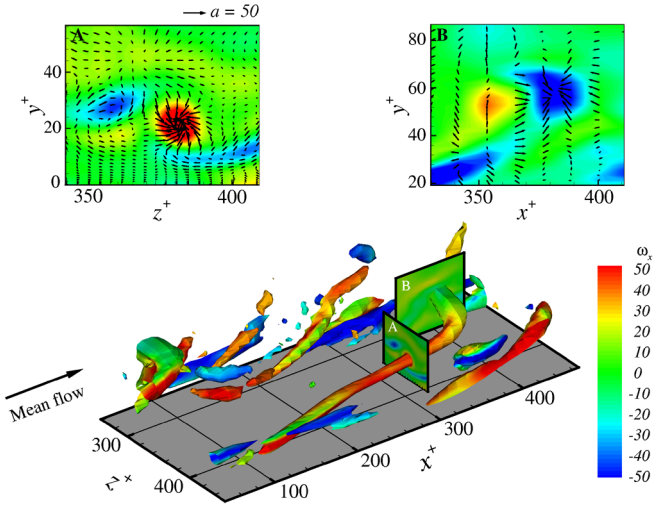

FIG. 3 (color online). Visualization of the near wall coherent vortical structures. The streamwise vortices and a hairpin vortex are recognizable. Contours on the surface of the structures denote the streamwise component of vorticity vector. In the y-z cross section of the leg of the hairpin vortex and in the x-z cross section of the head of the same vortex, color contours of the streamwise and spanwise components of vorticity are drawn with acceleration vectors.

structures (Fig. 3) strongly indicate that intermittently appearing accelerations of large magnitude are in large part associated with the coherent vortical structures in the form of the centripetal acceleration. To quantitatively investigate this, the angles between the pressure gradient, which is the major contributor to acceleration, vorticity vector, and gradient of squared vorticity known as local enstrophy, are defined as

$$\cos\alpha = \frac{-\nabla p \cdot \boldsymbol{\omega}}{|\nabla p||\boldsymbol{\omega}|}, \tag{2}$$

$$\cos\beta = \frac{-\nabla p \cdot \nabla(\boldsymbol{\omega} \cdot \boldsymbol{\omega})}{|\nabla p||\nabla(\boldsymbol{\omega} \cdot \boldsymbol{\omega})|}. \tag{3}$$

Acceleration data at $y^+ = 30$, where the near wall structures are typically found, are used to obtain the mean-squared pressure gradient conditional on α and β by employing the density estimation method using a Gaussian kernel [14].

The corresponding mean-squared pressure gradient is plotted as functions of α and β in Fig. 4, clearly showing dominant peaks at $\alpha = 90°$ and $\beta = 0°$, while the probability density distribution of β almost vanishes at $\beta = 0$ as shown in the inset of Fig. 4. This readily indicates that the negative pressure gradient, which is the irrotational component of acceleration, indeed, tends to be orthogonal to the vorticity axis and at the same time to be directed towards the core of vortical structures where vorticity typically has its local maximum value in a very intermittent manner. Therefore, Fig. 4 serves as quantitative

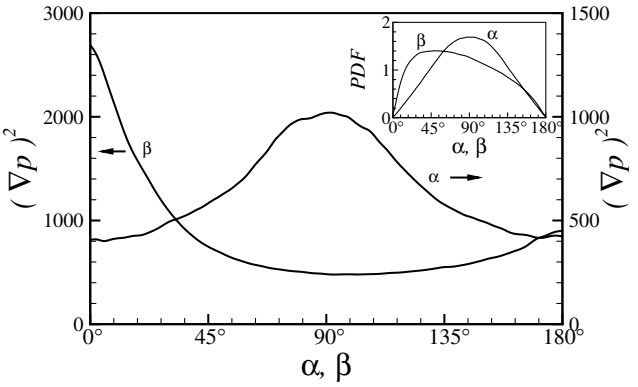

FIG. 4. The angles between the negative pressure gradient, vorticity vector, and the gradient of enstrophy defined by Eqs. (2) and (3) and the corresponding squared pressure gradient, at $y^+ = 30$. The corresponding probability density functions (PDFs) are shown in the inset.

evidence supporting that the intermittent acceleration of fluid particles is basically the centripetal acceleration associated with rotational motion of the near wall coherent vortical structures. It would be of much interest to investigate such a behavior for isotropic turbulence that has randomly distributed vortex tubes. In the previous studies on kinematic alignment [15–17], they investigated the angles between the pressure gradient and principal axes of strain rate tensors in isotropic turbulence and homogeneous shear turbulence. They found that near a vortex tube the most compressive and expansive principal axes are found mostly 45° from the pressure gradient vector. Considering that a vortex has irrotational strain around itself with two principal directions 45° from the radial direction, a similar trend is expected in isotropic turbulence.

Our finding is also consistent with the views of Mordant *et al.* [3] that long time correlation of the

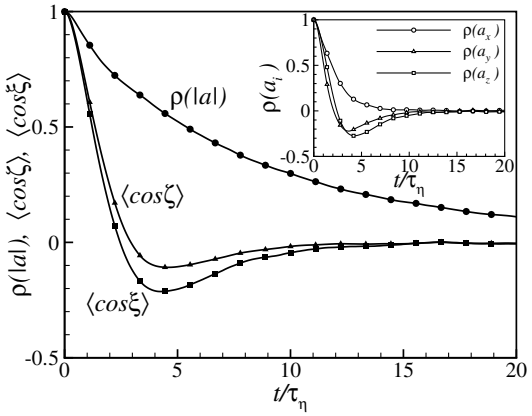

FIG. 5. The Lagrangian correlation of the magnitude of acceleration and the acceleration-magnitude-weighted mean of cosine of the angle defined by Eq. (4) of fluid particles released at $y^+ = 20$. In the inset, the Lagrangian correlation of each acceleration component is shown.

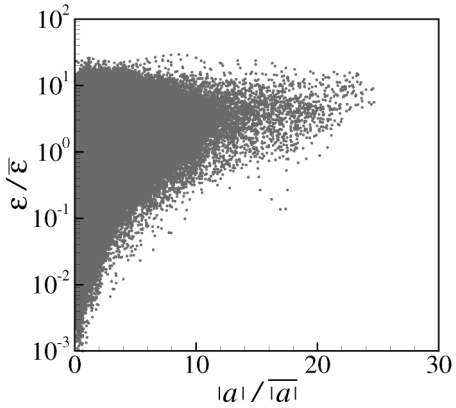

FIG. 6. Correlations between the magnitude of acceleration and the local dissipation at $y^+ = 20$.

magnitude of acceleration is a key element of intermittency since the centripetal acceleration of a particle trapped in a coherent structure preserves its magnitude longer than its direction. In Fig. 5, the Lagrangian correlation of the acceleration magnitude, the acceleration-magnitude-weighted mean of cosine of the angle ζ between vectors $\mathbf{a}(0)$ and $\mathbf{a}(t)$ defined by

$$\langle \cos\zeta \rangle = \frac{\overline{|\mathbf{a}(0)||\mathbf{a}(t)|\cos\zeta(t)}}{\overline{|\mathbf{a}(0)|}^{1/2}\overline{|\mathbf{a}(t)|}^{1/2}} \tag{4}$$

and the similarly weighted mean of the angle ξ, which is the projected angle of ζ onto the y-z plane are shown in terms of time normalized by the Kolmogorov time scale τ_η with acceleration correlation of each component in the inset. The zero crossing of the correlations of the wall-normal and spanwise accelerations at around two Kolmogorov time scales seems to be in large part a consequence of 90° rotation of the acceleration vectors projected onto the y-z plane.

Finally, we investigated the behavior of the rate of dissipation ϵ which has been believed to be related to intermittency of enstrophy [18]. We found that wherever large accelerations are observed, local dissipation is also strong. However, it is not the case in the other way; i.e., strong dissipation is not necessarily accompanied by large acceleration as shown in Fig. 6 where local dissipation 20 times larger than the mean dissipation is observed with all magnitudes of acceleration. Detailed investigation of flow fields reveals that local dissipation, which is a measure of irrotational strain, is strong not only in the very edge of the coherent rotational structures due to strong rotation but also in the region subject to irrotational strain between such rotational structures.

In summary, our simulation shows that acceleration in near wall turbulence is a very intermittent variable and the source of the intermittency is the near wall coherent vortical structures. Acceleration of a large magnitude is mainly the centripetal acceleration due to the rotational motion of fluid particles entangled in the near wall streamwise or hairpin-shaped vortices. Although our simulation was carried out for relatively low Reynolds numbers, considering the universal characteristics of the near wall coherent structures, it is likely that our finding is valid in high Reynolds number flows.

This research was supported by the Korea Science and Engineering Foundation through Grant No. R01-2003-000-10142-0. We thank J. Kim and A. M. Reynolds for helpful discussions.

*Electronic address: clee@yonsei.ac.kr
†Present address: Center for Environmental Medicine, Asthma and Lung Biology, University of North Carolina at Chapel Hill, Chapel Hill, NC 27599-7310, USA.

[1] A. La Porta, G. A. Voth, A. M. Crawford, J. Alexander, and E. Bodenschatz, Nature (London) **409**, 1017 (2001).
[2] G. A. Voth, A. La Porta, A. M. Crawford, J. Alexander, and E. Bodenschatz, J. Fluid Mech. **469**, 121 (2002).
[3] N. Mordant, J. Delour, E. Léveque, A. Arnéodo, and J.-F. Pinton, Phys. Rev. Lett. **89**, 254502 (2002).
[4] P. Vedula and P. K. Yeung, Phys. Fluids **11**, 1208 (1999).
[5] B. L. Sawford *et al.*, Phys. Fluids **15**, 3478 (2003).
[6] A. S. Monin and A. M. Yaglom, *Statistical Fluid Mechanics*, edited by J. L. Lumley (MIT Press, Cambridge, MA, 1975), Vol. 2.
[7] R. Gotoh and R. S. Rogallo, J. Fluid Mech. **396**, 257 (1999).
[8] Z.-S. She, E. Jackson, and S. A. Orszag, Nature (London) **344**, 226 (1990).
[9] J. Kim, P. Moin, and R. Moser, J. Fluid Mech. **177**, 133 (1987).
[10] J.-I. Choi, K. Yeo, and C. Lee, Phys. Fluids **16**, 779 (2004).
[11] R. J. Hill and S. T. Thoroddsen, Phys. Rev. E **55**, 1600 (1997).
[12] J. Jeong and F. Hussain, J. Fluid Mech. **285**, 69 (1995).
[13] S. K. Robinson, Annu. Rev. Fluid Mech. **23**, 601 (1991).
[14] B. W. Silverman, *Density Estimation for Statistics and Data Analysis* (Chapman & Hall, London, 1986).
[15] Wm. T. Ashurst, A. R. Kerstein, R. M. Kerr, and C. H. Gibson, Phys. Fluids **30**, 2343 (1987).
[16] Wm. T. Ashurst, J.-Y. Chen, and M. M. Rogers, Phys. Fluids **30**, 3293 (1987).
[17] J. Jiménez, Phys. Fluids A **4**, 652 (1992).
[18] B. W. Zeff *et al.*, Nature (London) **421**, 146 (2003).